



Fabrication and in vitro/vivo evaluation of quercetin nanocrystals stabilized by glycyrrhizic acid for liver targeted drug delivery

Baode Shen^{a,*}, Yuwen Zhu^{a,b,1}, Fengxia Wang^a, Xiang Deng^b, Pengfei Yue^a, Hailong Yuan^{b,*}, Chenying Shen^{c,*}

^a Key Laboratory of Modern Preparation of Traditional Chinese Medicine, Ministry of Education, Jiangxi University of Chinese Medicine, Nanchang 330004, China

^b Department of Pharmacy, Air Force Medical Center, PLA, Beijing 100142, China

^c Department of Pharmacy, Jiangxi Provincial People's Hospital, the First Affiliated Hospital of Nanchang Medical College, Nanchang 330006, China

ARTICLE INFO

Keywords:

Drug nanocrystals
Quercetin
Glycyrrhizic acid
Liver targeted drug delivery
Pharmacokinetics
Tissue distribution

ABSTRACT

The purpose of this study was to design novel drug nanocrystals (NCs) stabilized by glycyrrhizic acid (GL) for achieving liver targeted drug delivery due to the presence of GL receptor in the hepatocytes. Quercetin (QT) exhibits good pharmacological activities for the treatment of liver diseases, including liver steatosis, fatty hepatitis, liver fibrosis, and liver cancer. It was selected as a model drug owing to its poor water solubility. QT NCs stabilized by GL (QT-NCs/GL) were fabricated by wet media milling technique and systemically evaluated. QT-NCs stabilized by poloxamer 188 (QT-NCs/P188) were prepared as a reference for comparison of in vitro and in vivo performance with QT-NCs/GL. QT-NCs/GL and QT-NCs/P188 with similar particle size around 130 nm were successfully fabricated by wet media milling technique. Both of QT-NCs/GL and QT-NCs/P188 showed irregular particles and short rods under SEM. XRPD revealed that QT-NCs/GL and QT-NCs/P188 remained in crystalline state with reduced crystallinity. QT-NCs/GL and QT-NCs/P188 exhibited significant solubility increase and drug release improvement of QT as compared to raw QT. No significant difference for the plasma concentration–time curves and pharmacokinetic parameters of QT were found following intravenous administration of QT-NCs/GL and QT-NCs/P188. However, a significantly higher liver distribution of QT following intravenous administration of QT-NCs/GL was observed in comparison to QT-NCs/P188, indicating QT-NCs stabilized by GL could achieve liver targeted delivery of QT. It could be concluded that GL used as stabilizer of QT NCs have a great potential for liver targeted drug delivery.

1. Introduction

Over the past decades, nanocrystals (NCs) have received widespread attention as one of successful formulation strategies for improving bioavailability of insoluble drugs and natural products (Kalhapure et al., 2022; Ma et al., 2023; McGuckin et al., 2022). Drug NCs are pure drug crystalline nanoparticles stabilized by a small amount of stabilizer (surfactants and/or polymers), with an average particle size <1000 nm and typically ranging from 200 to 500 nm (Shen et al., 2016). Due to their small particle size and high specific surface area, NCs have remarkable advantages in improving the dissolution of insoluble drugs and enhancing their bioavailability (Gigliobianco et al., 2018; Mohammad et al., 2019; Tu et al., 2020). They also possess the outstanding properties of high drug loading, low toxicity, simple preparation

process, and wide application (Kalhapure et al., 2022; Ma et al., 2023; McGuckin et al., 2022; Shen et al., 2016). In the early development stages, NCs were primarily used to improve the oral bioavailability of drugs with poor water solubility (Gao et al., 2013), but they currently have been expanded to other various drug delivery systems including parenteral, transdermal, pulmonary, ocular and targeted drug delivery, etc (Jacob et al., 2020; Lu et al., 2022; Mohammad et al., 2019). Drug NCs with modified physicochemical properties for targeted drug delivery could maintain a potent therapeutic concentration to produce desirable pharmacological effect due to their high drug loading (Zingale et al., 2022).

Although only a small amount of stabilizer is used in NCs formulations, it is crucial to the formation and stability of NCs, as it can adsorb on the surface of nanoparticles during the NCs preparation, preventing

* Corresponding authors.

E-mail addresses: shenbaode@163.com (B. Shen), yhlpharm@126.com (H. Yuan), shenchengying0728@163.com (C. Shen).

¹ These authors contributed equally to this work.

nanoparticles aggregation and agglomeration through electrostatic repulsion and/or steric hindrance, thereby maintaining the stability of NCs (Li et al., 2021; Yang et al., 2018). Selection and optimization of stabilizers and their concentrations are important for the successful formulation and stabilization of NCs (Jacob et al., 2020). Generally, stabilizers are selected based on the requirement of particle size and physical stability during the preparation of drug NCs (Tuomela et al., 2016). So far, commonly stabilizers used for drug NCs mainly include surfactants and polymers (Li et al., 2021). In addition, food proteins (soybean protein isolate, whey protein isolate and β -lactoglobulin) (Aditya et al., 2015; He et al., 2013), serum proteins (albumin and transferrin) (Lu et al., 2014; Yin et al., 2016) and natural saponins (glycyrrhizin, panax notoginseng saponins and tea saponins) (Hang et al., 2021; Jin et al., 2019; Long et al., 2020) were also explored as alternative stabilizers for drug NCs.

Notably, some stabilizers can maintain the stability of drug NCs, while also affect the in vivo performances of drug NCs (Qin et al., 2022; Soisuwan et al., 2019), which can be considered as functional stabilizers. Moreover, active targeted drug delivery can be achieved via surface modification of drug NCs by functional stabilizers with the ability to specifically target surface receptors (Lu et al., 2022; Zingale et al., 2022), as drug NCs were demonstrated to be long biological life in the body following intravenous delivery (Hang et al., 2022; Shen et al., 2021a; Wang et al., 2018). Transferrin modified docetaxel NCs significantly improved the cellular uptake and cytotoxicity of docetaxel in A549 cell line via interacting with transferrin receptors that are higher expressed in cancer cells, achieving tumor targeting drug delivery (Choi and Park, 2017). Combination of tween 80 and TPGS was demonstrated to be viable stabilizer for surface modification of baicalin NCs that could improve baicalin access to the brain through adsorbing apolipoprotein and repelling opsonin adsorption (Liu et al., 2017).

Glycyrrhizin acid (GL), a triterpenoid saponin obtained from licorice, possesses numerous pharmacological effects including anti-inflammatory, immunomodulatory, hepatoprotective, antiviral, and antitumor activities, etc (Chen et al., 2020; Selyutina and Polyakov, 2019). GL has been also used as multifunctional carrier to improve bioavailability of drugs with low water solubility or poor membrane permeability as it is able to increase the membrane fluidity and permeability by incorporation into the lipid bilayer (Selyutina and Polyakov, 2019; Shen et al., 2021b; Yang et al., 2015). In our previous study, GL was demonstrated to be a novel stabilizer of drug NCs for enhancing bioavailability and synergistic hepatoprotective effect due to the dual-property of surfactant stabilizer and active pharmaceutical ingredient (Hang et al., 2021). More importantly, due to the presence of specific receptors in the hepatocytes, GL and its hydrolyzed metabolite glycyrrhetic acid were served as specific ligands for liver targeting nanosystems (Stecanella et al., 2021), such as liposomes, polymeric nanoparticles and nanogels (Zhao et al., 2021a). However, no study was reported the application of GL as stabilizer of drug NCs for liver targeted delivery.

Therefore, the present study was performed to design a novel drug NCs stabilized by GL for liver targeted drug delivery. Quercetin (QT), a natural flavonoid, exhibits good pharmacological activities for the treatment of liver diseases, including liver steatosis, fatty hepatitis, liver fibrosis, and liver cancer (Zhao et al., 2021b). It was selected as a model drug owing to its poor water solubility. QT NCs stabilized by GL (QT-NCs/GL) were prepared by wet media milling technique and systematically investigated its physicochemical properties by dynamic light scattering (DLS), scanning electron microscopy (SEM), X-ray powder diffractometry (XRPD) and differential scanning calorimetry (DSC). The solubility and in vitro drug release behavior of QT-NCs/GL were also examined. In order to evaluate the liver-targeting potential of QT-NCs/GL, the pharmacokinetics and tissue distribution of QT were investigated in rats following intravenous administration of QT-NCs/GL. All tests were performed with QT-NCs stabilized by poloxamer 188 (QT-NCs/P188) serving as a reference for comparison.

2. Materials and methods

2.1. Materials

Quercetin (purity >98%) was provided by Shanxi Ciyuan Biotechnology Co., Ltd. (Shanxi, China). Glycyrrhizic acid (purity >95%) was provided by Beijing Century Aoke Biotechnology Co., Ltd. (Beijing, China). Poloxamer 188 was provided by Beijing Fengli Jingqiu Trading Co., Ltd. (Beijing, China). Kaempferol (purity >98%) was provided by Chengdu Pufeide Biotechnology Co., Ltd. (Chengdu, China). HPLC-grade methanol was provided by Fisher Scientific (MA, USA). All other reagents were of analytical grade.

2.2. Preparation of QT-NCs

QT-NCs were prepared using the wet media milling technique (Hang et al., 2021). Initially, the stabilizer solution was formed by dissolving GL in deionized water and then 4 mL of stabilizer solution transferred into a 10 mL glass vial used as a milling chamber. Subsequently, after adding 4 mL of yttrium stabilized zirconia beads with a diameter of 0.4–0.6 mm, 40 mg of QT was dispersed in stabilizer solution in the milling chamber and then milled by magnetic stirring (DF101D, Gongyi Yuhua instrument Co, Ltd., Gongyi, China) at a controlled temperature of 25 °C. To obtain QT-NCs/GL with desired particle size and stability, the mass ratio of QT to GL (10:1, 10:2, 10:3, 10:4, 10:5), milling speed (600, 800, 1000, 1200 rpm), and milling time (0.5, 1, 2, 4 h) were optimized with particle size (PS), polydispersity index (PDI), and stability index (SI) as key evaluation metrics.

In addition, QT-NCs/P188 with same formulation to the optimized QT-NCs/GL were prepared to obtain similar particle size by controlling the milling time.

2.3. Characterization of QT-NCs

2.3.1. Size distribution and zeta potential analysis

The size distributions of QT-NCs/GL and QT-NCs/P188 were respectively analyzed by DLS using Winner 801 nanoparticle size analyzer (Jinan Winner Particle Instrument Stock Co., Ltd. China) at 25 °C after 100-fold dilution with deionized water and expressed as particle size (intensity mean) and PDI. Their zeta potential was determined using a JS94H zeta potential analyzer (Shanghai Zhongchen Digital Technic Apparatus Co., Ltd., China) at a constant temperature of 25 °C. Each sample was measured in triplicate.

2.3.2. Stability index

The stability index (SI) was used to evaluate the stability of QT-NCs. SI was calculated according to the literature method (Yue et al., 2013) with a modification, as follows:

$$SI(\%) = \frac{PS_c}{PS_0} \times 100\%$$

where PS_0 represents the mean particle size value of QT-NCs before centrifugation and PS_c is the corresponding particle size value of unprecipitated QT-NCs after centrifugation at 3000 rpm for 15 min. Drug NCs with SI value of near 100% usually mean more stable (Yue et al., 2013).

2.3.3. SEM

The morphological evaluation of raw QT, QT-NCs/GL and QT-NCs/P188 was conducted using an S-4800 scanning electron microscope (Hitachi, Ltd., Tokyo, Japan). After appropriate dilution with deionized water, QT-NCs samples were dropped onto tin-foil paper, dried at room temperature, followed by gold coating and images were captured using SEM at an excitation voltage of 5 kV.

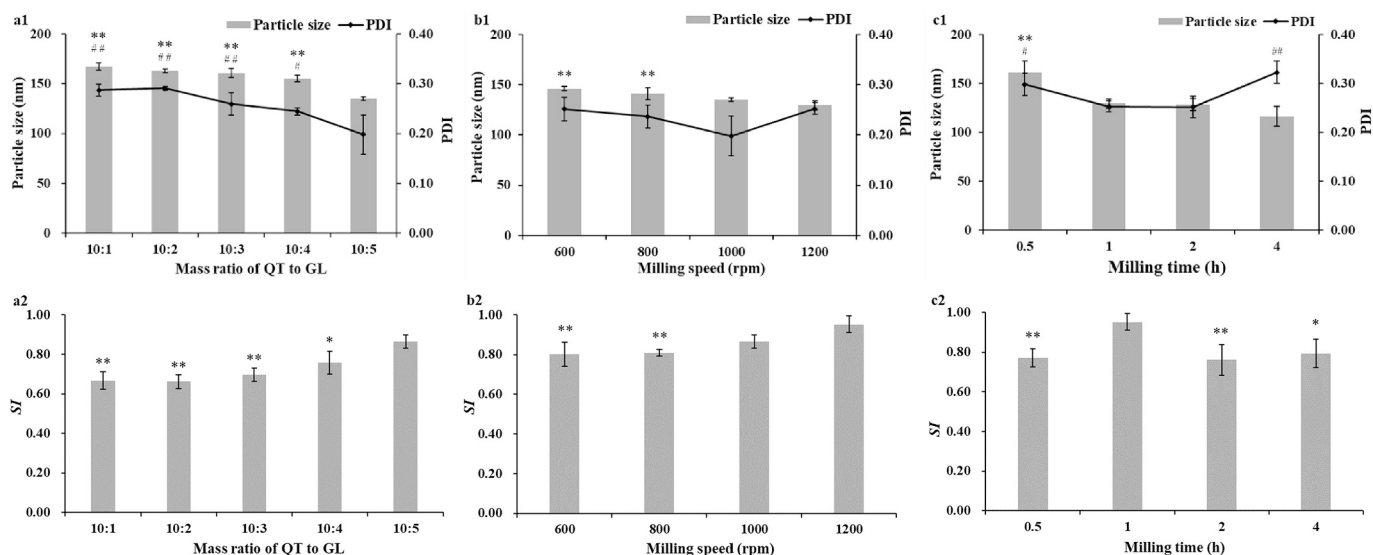


Fig. 1. Effects of mass ratio of QT to GL (a), milling speed (b) and milling time (c) on particle size, PDI and *SI* of QT-NCs/GL and QT-NCs/P188. (mean \pm SD, $n = 3$; Particle size: a1. ** $P < 0.01$ versus 10:5, b1. ** $P < 0.01$ versus 1200 rpm, c1. ** $P < 0.01$ versus 1 h; PDI: a1. # $P < 0.05$, ## $P < 0.01$ versus 10:5, b1. # $P < 0.05$ versus 1200 rpm; c1. # $P < 0.05$, ## $P < 0.01$ versus 1 h; *SI*: * $P < 0.05$, ** $P < 0.01$ versus 10:5, b1. ** $P < 0.01$ versus 1200 rpm, c1. * $P < 0.05$, ** $P < 0.01$ versus 1 h.)

2.3.4. XRPD and DSC

QT-NCs/GL and QT-NCs/P188 were dried using lyophilization (FD5, Gold SIM, Beijing, China) without the addition of cryoprotectants for XRPD and DSC analysis. The XRPD patterns of raw QT, QT-NCs/GL and QT-NCs/P188 were recorded by a D8 X-ray diffractometer (Advance, Karlsruhe, Germany) running in step scan mode with Cu source of radiation at 40 kV voltage and 25 mA current over the 2θ range of $3^\circ \sim 60^\circ$ at a scanning rate of $2^\circ/\text{min}$. DSC measurements of the same samples were performed using a thermal analyzer (DSC200F3, Netzsch, Selb, Germany). Approximately 5 mg of each sample was analyzed in open aluminum pans and heated at the speed of $10^\circ\text{C}/\text{min}$ from 40°C to 350°C under nitrogen atmosphere.

2.4. Solubility determination

For solubility determination, excessive powder samples of crude QT, the physical mixtures of QT and stabilizers, and QT-NCs, with equal amount of QT, were dispersed in deionized water and shaken using a mechanical water bath shaker (Shandong Boke Scientific Instruments Co. Ltd., China) at 25°C for 48 h. After centrifugation at 10000 rpm for 30 min, the supernatant was filtered through 50 nm filters (Sigma-Aldrich, St Louis, MO, USA) and analyzed by HPLC method with an LC-20 CE HPLC system (Shimadzu Corp, Kyoto, Japan). An InterSustain C_{18} column ($250 \times 4.6 \text{ mm}, 5 \mu\text{m}$) with column temperature kept at 30°C and mobile phase of methanol/0.1% phosphoric acid solution (59:41, v/v) at a flow rate of 1 mL/min were used for chromatographic separation. The sample injection volume was 20 μL and the detection wavelength was 375 nm.

2.5. In vitro drug release test

The in vitro drug release of QT-NCs/GL was compared with raw QT and QT-NCs/P188 by the paddle method described in Chinese Pharmacopeia 2020 using ZRS-8G dissolution tester (TDTF Technology Limited., Tianjin, China). The phosphate buffer solution (PBS, pH 7.4) containing 0.1% (w/v) tween 80 was used as dissolution medium (Qiao et al., 2020). Raw QT powder, and lyophilized powder of QT-NCs/GL and QT-NCs/P188, equivalent to 3 mg of QT, were respectively added to 250 mL of dissolution medium at a temperature of $(37.0 \pm 0.5)^\circ\text{C}$ with the rotation speed of the paddle at 100 rpm. 2 mL of samples was taken at predefined time intervals and concurrently replenished by an

equal volume of dissolution medium. Each sample was filtrated through 50 nm filters and analyzed by the same HPLC method as described in Section 2.4. All tests were performed in triplicate.

2.6. Pharmacokinetics and tissue distribution studies

2.6.1. Animals

Male Sprague Dawley (SD) rats weighing 180–220 g were obtained from SPF (Beijing) Biotechnology Co., Ltd. (Beijing, China) and kept in a breeding room with controlled environments ($25 \pm 1^\circ\text{C}$, $50 \pm 10\%$ relative humidity and 12 h light-dark cycle). The rats were given free access to food and water. All experiments were carried out strictly in accordance with the NIH Guidelines for the Care and Use of Laboratory Animals and approved by the Institutional Ethics Committee of Air Force Medical Center, PLA of China (No. 2023–58-PJ01).

2.6.2. Pharmacokinetics

All rats were adaptively raised for 3 days and fasted for 12 h before experiments. Twelve SD rats were randomly divided into two groups of six animals per group and respectively received QT-NCs/GL and QT-NCs/P188 at a dose of 50 mg/kg QT via injection through the tail vein. About 0.5 mL of blood samples were collected into heparinized tubes from the orbital venous plexus at 0.083, 0.25, 0.5, 1, 2, 4, 6, 8, 12 and 24 h after drug administration. The obtained blood samples were immediately centrifuged at 5000 rpm for 10 min and the plasma samples were gathered and stored at -20°C until analysis.

2.6.3. Tissue distribution

Forty-eight male SD rats were used for tissue distribution studies. Animal grouping and drug administration were the same as described in Section 2.7.1. Three rats were sacrificed at each time point of 0.083, 0.5, 1, 2, 4, 8, 12, and 24 h postdosing and various organs were dissected after cardiac perfusion with physiological saline. All collected organs were gently rinsed with physiological saline to remove residual blood, dried with tissue paper and stored at -20°C until analysis.

2.6.4. Plasma and tissue sample analysis

The collected organs were accurately weighed, and homogenized after addition of 2 times the volume of physiological saline. Both of plasma and tissue homogenates processed by modified acid-hydrolyzed method for QT extraction following our previous reports (Shen et al.,

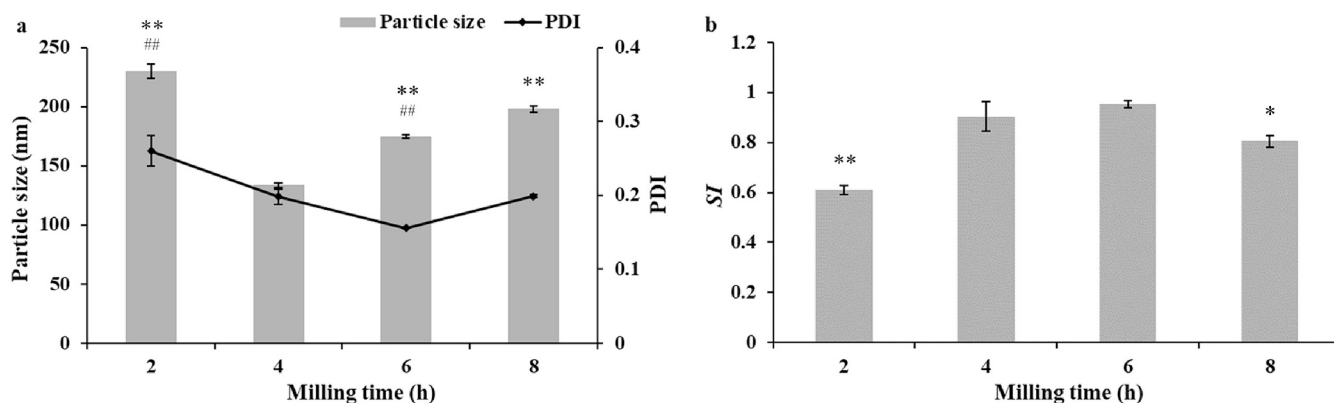


Fig. 2. Effect of milling time on particle size, PDI and *SI* of QT-NCs/P188. (mean \pm SD, $n = 3$; a. Particle size: ** $P < 0.01$ versus 4 h; PDI: ## $P < 0.01$ versus 4 h; b. *SI*: * $P < 0.05$, ** $P < 0.01$ versus 4 h.)

2021a; Wang et al., 2022) and analyzed by the same HPLC method as described in Section 2.4., with kaempferol as an internal standard.

2.7. Statistical analysis

All data are expressed as the mean \pm standard deviation (SD). The pharmacokinetic parameters were calculated by DAS2.0 software (Boying Corporation, Beijing, China) with noncompartmental model. Student's *t*-test was used for statistical analysis and comparing difference between the experimental groups with $P < 0.05$ as statistical significance.

3. Results and discussion

3.1. Fabrication of QT-NCs

In this study, wet media milling method was adopted for QT-NCs/GL fabrication, as it is an eco-friendly fabrication method with no organic solvent and easy to scale up (Mohammad et al., 2019). Drug NCs with smaller particle size is usually desired, therefore, the mass ratio of QT to GL, milling speed and milling time were optimized to obtain QT-NCs/GL with desired size distribution. The results are shown in Fig. 1. Fig. 1 a1 and a2 showed that the particle size, PDI and *SI* were significantly influenced by the mass ratio of QT to GL. Both particle size and PDI decreased, while *SI* increased, along with the rise of the mass ratio of QT to GL. When the mass ratio of QT to GL was 10:5, the particle size and PDI of QT-NCs/GL were significant lower and *SI* value was remarkable higher as compared to that of other mass ratios. It's not difficult to speculate from our results that further increasing the mass ratio of QT to GL may result in a further reduction in particle size. However, GL is not well dissolved in water and gelation would be happened with excessive amount of GL in water (Hang et al., 2021; Tucker et al., 2021), which adversely affects the fabrication of QT-NCs/GL. Thus, a mass ratio of 10:5 for QT to GL was selected as the suitable formulation for QT-NCs/GL fabrication.

The effects of milling speed and milling time on particle size, PDI and *SI* of QT-NCs/GL are shown in Fig. 1 (b1, b2 and c1, c2). Milling speed showed no significant effect on the PDI of QT-NCs/GL, but remarkably affect the particle size and *SI* of QT-NCs/GL (Fig. 1 b1 and b2). As milling speed increased from 600 rpm to 1000 rpm, the particle size of QT-NCs/GL significantly decreased and *SI* increased markedly, but only a slight decrease for particle size and a slight increase for *SI* without significant difference was observed with further increase of milling speed to 1200 rpm. The increase in milling time from 0.5 h to 1 h resulted in significant reduction for particle size and PDI of QT-NCs/GL, while a slight decrease for particle size without significant difference and significant increase for PDI was observed with further prolonging milling time from 1 h to 4

Table 1

Particle size, PDI, *SI* and zeta potential of QT-NCs/GL and QT-NCs/P188 (mean \pm SD, $n = 3$).

	QT-NCs/GL	QT-NCs/P188
Particle size (nm)	129 \pm 5	134 \pm 2
PDI	0.253 \pm 0.011	0.198 \pm 0.011
<i>SI</i>	0.952 \pm 0.042	0.903 \pm 0.129
Zeta potential (mV)	-33.8 \pm 2.9	-18.5 \pm 2.2

h (Fig. 1c1). A higher *SI* value was found at milling time of 1 h as compared to other milling time (Fig. 1c2). Considering the results of particle size and *SI*, the milling speed and milling time were determined to be 1000 rpm and 1 h, respectively.

P188, as one of most common poloxamers utilized in drug NCs, was used for QT-NCs preparation in our previous study (Shen et al., 2021a). Therefore, QT-NCs/P188 were fabricated as a reference for comparison of in vitro and in vivo performance with QT-NCs/GL, especially for the comparison of liver distribution, to verify the potential of QT-NCs/GL for liver targeted drug delivery. In order to eliminate the potential interference of fabrication methods and stabilizer concentration, QT-NCs/P188 were prepared via wet media milling method with the mass ratio of QT to GL fixed at 10:5, and the milling time was optimized to obtain QT-NCs/P188 with similar particle size to QT-NCs/GL (Fig. 2). The particle size and PDI of QT-NCs/P188 firstly decreased and then increased with significant difference as the milling time increased from 2 h to 8 h. And a higher *SI* value was observed at milling time of 4 h as compared to the milling time of 2 h and 8 h. Finally, the milling time of QT-NCs/P188 was set as 4 h.

3.2. Characterization of QT-NCs

QT-NCs/GL and QT-NCs/P188 with similar particle size around 130 nm were successfully fabricated by wet media milling method (Table 1). A relatively narrow size distribution can be found for QT-NCs/GL and QT-NCs/P188 (Fig. 3A), evidenced by the PDI values < 0.3 . The physical stability of QT-NCs/GL and QT-NCs/P188 were preliminary estimated by determination of zeta potential and *SI*. Generally, nanoparticles with higher absolute zeta potential value (above 30 mV) have relatively good physical stability as the sufficient electric repulsion between each particle provided by high surface charge could prevent nanoparticles from aggregation and agglomeration (Guo et al., 2013; Shen et al., 2013). QT-NCs/GL exhibited a high zeta potential of -33.8 ± 2.9 mV, indicating its good physical stability, which was further confirmed by the high *SI* value of 0.952 ± 0.042 . QT-NCs/P188 displayed a low zeta potential of -18.5 ± 2.2 , but a high *SI* value of 0.903 ± 0.129 , which may be attributed to the steric stabilization effect due to the formation of the

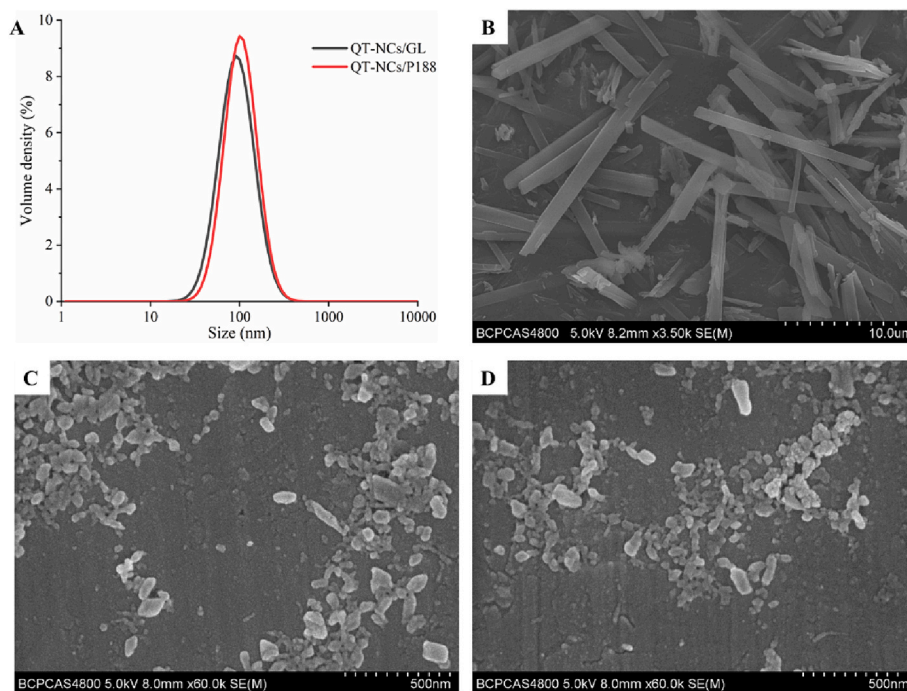


Fig. 3. Size distribution (A) and SEM images of raw QT (B), QT-NCs/GL (C) and QT-NCs/P188 (D).

steric layer between the nanoparticles created by polymeric chains of P188 on the nanoparticle surfaces (Tuomela et al., 2016).

The morphology of QT-NCs/GL and QT-NCs/P188 were evaluated by SEM and compared with that of raw QT. As shown in Fig. 3B, QT exhibited a distinct rod-shaped crystalline structure with obvious edges and corners, and its particle size was around 10–40 μm with uneven distribution. Both of QT-NCs/GL and QT-NCs/P188 showed irregular particles and short rods with the estimated average sizes in the range of 100–300 nm (Fig. 3C and D), which is consistent with the results of particle size analysis. Significant changes have occurred in both morphology and particle size of QT via wet media milling. This was mainly because the raw QT particles are broken down via bead collision during milling process (Tian et al., 2022).

The crystalline state of QT-NCs/GL and QT-NCs/P188 were compared by XRPD and DSC analysis. As shown in Fig. 4A, QT exhibited characteristic diffraction peaks at 2θ values of 10.6°, 12.3°, 15.6°, 24.2° and 27.2°, indicating its crystalline nature, which is in accordance with our previous studies (Shen et al., 2018; Wang et al., 2022). The characteristic diffraction peaks of QT at 2θ values around 10° and 27° were also found in the XRPD spectra of QT-NCs/GL and QT-NCs/P188, suggesting that QT-NCs still remained in a crystalline state. However, the peaks intensities were very low and some characteristic diffraction peaks even disappeared in the XRPD spectra of QT-NCs/GL and QT-NCs/P188, indicating reduced crystallinity. In addition, P188 showed two weak diffraction peaks in the 2θ values range of 18°–25° and GL was found a weak diffraction peak at 2θ value around 14° in our previous reports (Shen et al., 2018; Shen et al., 2020), but no characteristic diffraction peaks for GL or P188 were observed in the XRPD spectra of QT-NCs/GL or QT-NCs/P188. The change of XRPD spectra could be attributed to the effect of nanomilling and the interactions between drug and stabilizers. These results also demonstrated that the combination of nanomilling process and stabilizer (GL or P188) addition have no influence on the crystalline state of QT, but might reduce its crystallinity.

The DSC diagram shows similar results to the XRPD spectra. Two endothermic peaks were found in the DSC curve of QT (Fig. 4B), which was in agreement with our previous report (Shen et al., 2018). The first endothermic peak between 100 °C and 150 °C was corresponding to the loss of bound water, while the sharp peak at around 320 °C ascribed to

the melting point of QT. Both of QT-NCs/GL and QT-NCs/P188 displayed a weak endothermic peak at around 300–310 °C, further confirming their crystalline nature. The endothermic peak for QT-NCs/GL and QT-NCs/P188 shifted to the left as compared to that of QT, which may be attributed to the nanosize effect leading to a decrease in melting point. GL exhibited an endotherm peak around 225 °C in our previous report (Shen et al., 2020), but no endotherm peak of GL was found in the QT-NCs/GL. The effect of nanomilling and the interactions between drug and stabilizers as proposed in XRPD study can also be employed to interpret this phenomenon.

3.3. Solubility and *in vitro* drug release

The QT concentrations in deionized water and dissolution medium were determined by HPLC method with same methodological validation parameters. The standard curve of QT was obtained by taking the peak area of QT (y) as the ordinate and the concentration of QT (x) as the abscissa. Within the concentration range of 4.00–40.00 $\mu\text{g}/\text{mL}$, a good linear relationship between y and x was observed, with the regression equation of QT was $y = 71,939x + 4816.1$ and a regression coefficient of $R^2 = 0.9999$. The mean recovery of QT ranged from 98.07% to 100.88% ($n = 9$), and the intra- and inter-day precisions were below 2%.

The solubility of QT was only $0.33 \pm 0.04 \mu\text{g}/\text{mL}$, while the solubility was determined to be $22.31 \pm 1.07 \mu\text{g}/\text{mL}$ for QT-NCs/P188 and $52.94 \pm 4.30 \mu\text{g}/\text{mL}$ for QT-NCs/GL. The solubility of QT-NCs/P188 and QT-NCs/GL was increased by about 67 and 160 times, respectively, as compared to raw QT, but only a slight solubility increase was observed for their physical mixture ($1.25 \pm 0.17 \mu\text{g}/\text{mL}$ for the physical mixture of QT and GL, $0.41 \pm 0.07 \mu\text{g}/\text{mL}$ for the physical mixture of QT and P188). Therefore, the reduction of the particle size into the nanosize range is the main contribution for QT solubility increase (Dhaval et al., 2020).

The drug release profiles of QT-NCs/GL, QT-NCs/P188, and raw QT are presented in Fig. 5. The release of QT from QT-NCs/GL and QT-NCs/P188 was significantly improved as compared to raw QT. Only 31.22% of QT was released from raw QT within 60 min, while the cumulative release of QT from QT-NCs/GL and QT-NCs/P188 were 74.27% and 68.31%, respectively. According to the Noyes–Whitney equation and the

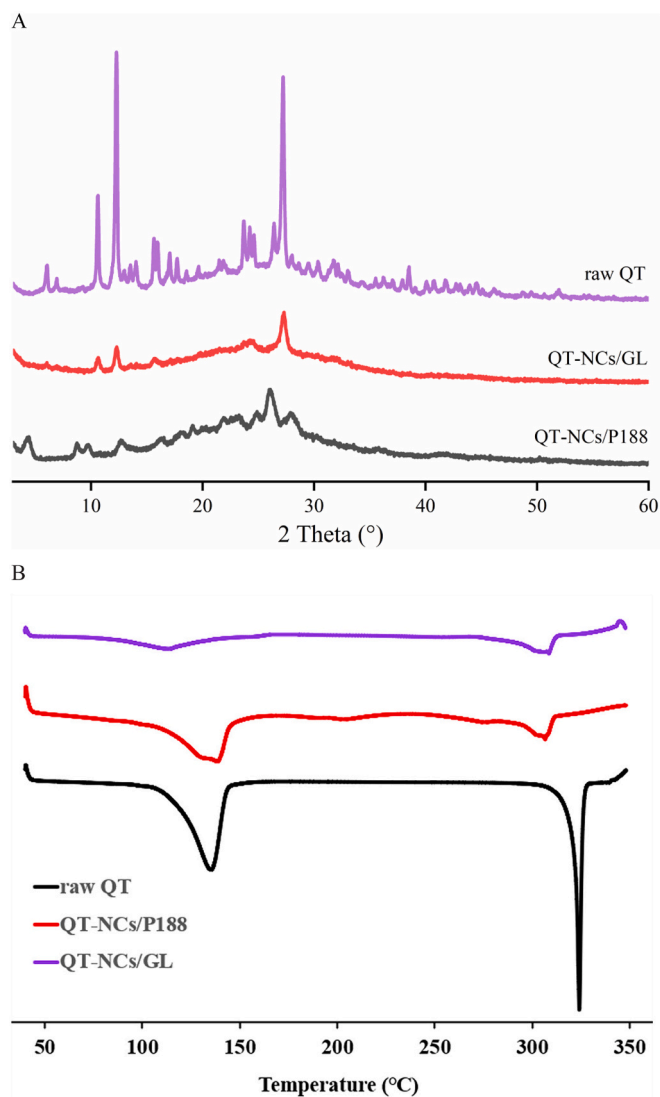


Fig. 4. XRPD patterns (A) and DSC thermograms (B) of raw QT, QT-NCs/GL and QT-NCs/P188.

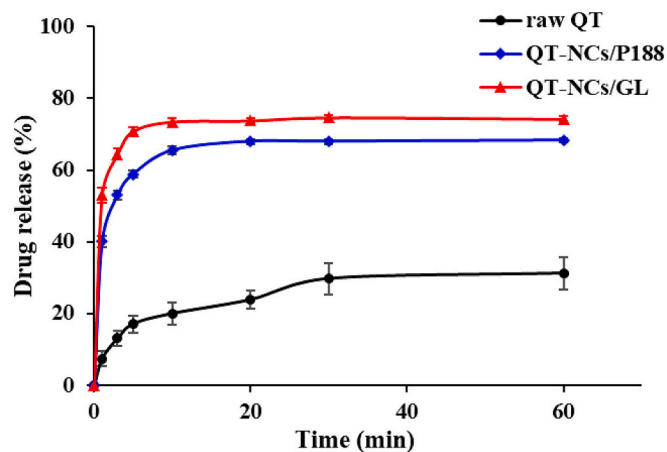


Fig. 5. In vitro drug release profiles of QT-NCs/GL, QT-NCs/P188 and raw QT (mean \pm SD, n = 3).

Table 2

Linear regression equations of QT in plasma and tissue homogenates.

Samples	regression equations	R ²	Linear range ($\mu\text{g/mL}$)
Plasma	$y = 0.0331x - 0.006$	1.0000	0.25–150.00
Heart	$y = 0.1292x + 0.0147$	0.9999	0.25–25.00
Liver	$y = 0.1578x - 0.0203$	0.9999	0.25–100.00
Spleen	$y = 0.1496x + 0.0051$	0.9996	0.25–50.00
Lung	$y = 0.1476x + 0.0188$	0.9998	0.25–50.00
Kidney	$y = 0.1396x - 0.0063$	1.0000	0.25–50.00

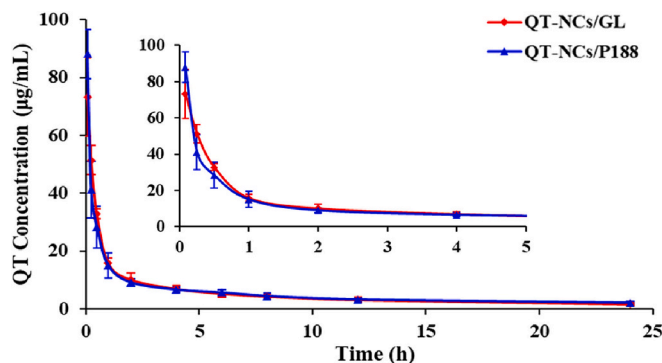


Fig. 6. Plasma concentration–time curves of QT after intravenous administration of QT-NCs/GL and QT-NCs/P188 (mean \pm SD, n = 6).

Table 3

The main pharmacokinetic parameters of QT after intravenous administration of QT-NCs/GL and QT-NCs/P188 (mean \pm SD, n = 6).

	QT-NCs/GL	QT-NCs/P188
AUC _{0–t} ($\mu\text{g/mL}\cdot\text{h}$)	139.49 \pm 16.29	133.82 \pm 16.62
MRT _{0–t} (h)	6.32 \pm 0.43	7.06 \pm 0.58
C _{max} ($\mu\text{g/mL}$)	51.46 \pm 5.04	41.23 \pm 9.77
t _{1/2z} (h)	10.90 \pm 4.21	10.46 \pm 2.20

Prandtl equation, the improvement of QT release achieved by NCs formulations could be explained as follows: the significant particle size reduction of drug NCs creates high surface area in contact with the dissolution medium and simultaneously decrease the distance of diffusion layer around the drug particles, thereby resulting in high drug release (Dhaval et al., 2020; Junyaprasert and Morakul, 2015).

3.4. Pharmacokinetics and tissue distribution

The QT concentrations in plasma and tissue homogenates were determined by same HPLC method with different methodological validation parameters. The standard curves of QT in plasma and tissue homogenates were obtained by taking the concentration of QT (x) as the abscissa and the peak area ratio (y) of QT to kaempferol as the ordinate. The regression equations of QT for plasma and tissue homogenates are shown in Table 2, suggesting good linear relationships between y and x. The mean recovery of QT in plasma and tissue homogenates is 86.26% \sim 106.43%, with RSD < 5%. The intra- and inter-day precisions are < 8%.

The plasma concentration–time curves of QT after intravenous administration of QT-NCs/GL and QT-NCs/P188 are shown in Fig. 6, and the corresponding pharmacokinetic parameters are displayed in Table 3. No significant difference for the plasma concentration–time curves and pharmacokinetic parameters of QT were found following intravenous administration of QT-NCs/GL and QT-NCs/P188, suggesting that QT-NCs/GL exhibited equivalent pharmacokinetic performances in comparison to QT-NCs/P188.

The biodistribution of QT after intravenous administration of QT-

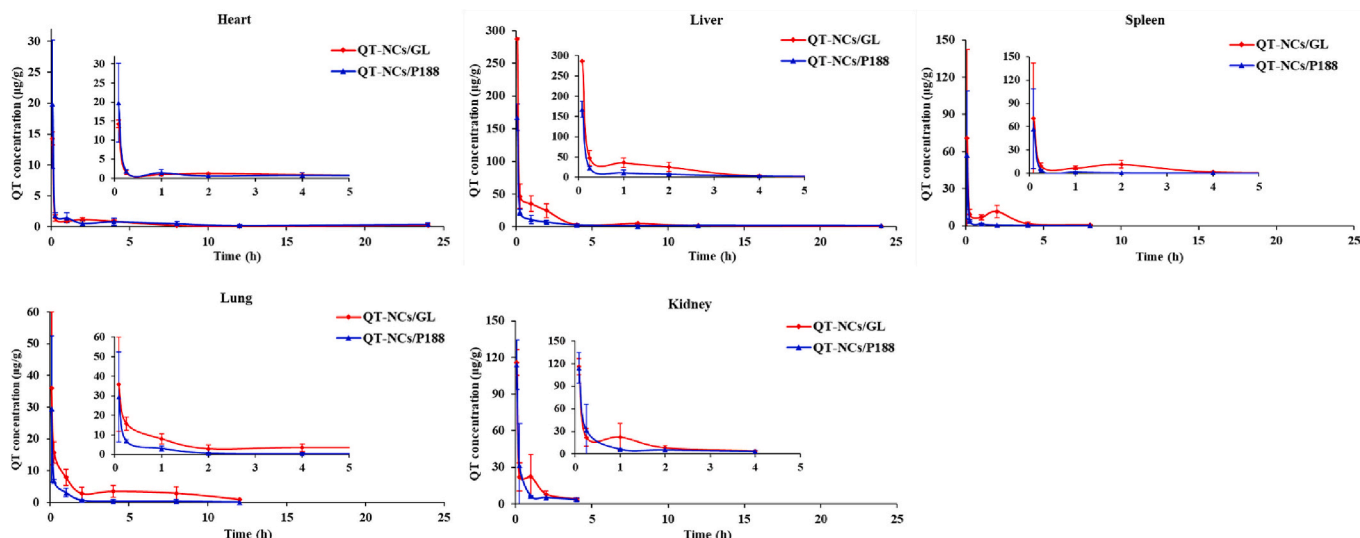


Fig. 7. Mean QT concentration-time profiles in main organs after intravenous administration of QT-NCs/GL and QT-NCs/P188 (mean \pm SD, n = 3).

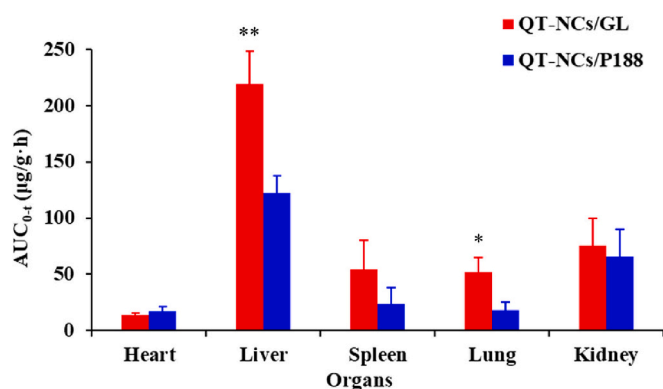


Fig. 8. The AUC_{0-t} of the QT distribution in different organs after intravenous administration of QT-NCs/GL and QT-NCs/P188 (mean \pm SD, n = 3). * $P < 0.05$, ** $P < 0.01$ versus QT-NCs/P188.

NCs/GL and QT-NCs/P188 were compared. As shown in Fig. 7, both of QT-NCs/GL and QT-NCs/P188 showed rapidly distribution of QT to various organs with the maximum QT concentration in liver and the minimum QT concentration in heart at 5 min after intravenous administration. Fig. 8 displayed the AUC_{0-t} of QT for different organs following intravenous administration of QT-NCs/GL and QT-NCs/P188. Compared with QT-NCs/P188, a significantly higher liver distribution of QT following intravenous administration of QT-NCs/GL was observed. The presence of specific receptors for GL and its metabolite in the hepatocytes may contribute to the enhanced liver distribution of QT-NCs/GL (Stecanella et al., 2021; Zhao et al., 2021a). These results demonstrated that QT-NCs/GL could achieve liver targeted delivery of QT. Interestingly, a significantly enhanced lung distribution of QT was also found for QT-NCs/GL as compared to that of QT-NCs/P188, indicating its potential of lung targeted drug delivery. A possible explanation for the enhanced lung distribution of QT-NCs/GL is that GL could improve cellular uptake of drug by enhancing the permeability of cell membranes and influencing drug transporter in lung.

4. Conclusion

In this study, a novel QT-NCs/GL was designed for liver targeted drug delivery. QT-NCs/GL with particle size around 130 nm were successfully fabricated by wet media milling technique. QT-NCs/P188 were

also prepared as a reference for comparison of in vitro and in vivo performance with QT-NCs/GL. Both of QT-NCs/GL and QT-NCs/P188 showed irregular particles and short rods under SEM. XRPD and DSC revealed that QT-NCs/GL and QT-NCs/P188 remained in crystalline state with reduced crystallinity. QT-NCs/GL and QT-NCs/P188 exhibited significant solubility increase and drug release improvement of QT as compared to raw QT. No significant difference for the plasma concentration-time curves and pharmacokinetic parameters of QT were found following intravenous administration of QT-NCs/GL and QT-NCs/P188. However, a significantly higher liver distribution of QT following intravenous administration of QT-NCs/GL was observed in comparison to QT-NCs/P188, indicating QT-NCs/GL could achieve liver targeted delivery of QT. These results demonstrated that GL used as stabilizer of QT NCs have a great potential for liver targeted drug delivery.

Funding

This work was supported by the Science and Technology Research Project of Jiangxi Provincial Education Department (GJJ211262), and the Doctoral Research Startup Foundation of Jiangxi University of Chinese Medicine (2021BSZR025), and the National Natural Science Foundation of China (81803741), and Jiangxi University of Chinese Medicine Science and Technology Innovation Team Development Program (CXTD22006).

CRediT authorship contribution statement

Baode Shen: Writing – review & editing, Writing – original draft, Funding acquisition, Formal analysis, Conceptualization. **Yuwen Zhu:** Writing – original draft, Methodology, Investigation, Formal analysis. **Fengxia Wang:** Methodology, Investigation. **Xiang Deng:** Investigation. **Pengfei Yue:** Funding acquisition, Conceptualization. **Hailong Yuan:** Writing – review & editing, Conceptualization. **Chenyang Shen:** Writing – review & editing, Funding acquisition, Conceptualization.

Declaration of competing interest

The authors have no relevant financial or non-financial interests to disclose.

Data availability

Data will be made available on request.

References

- Aditya, N.P., Yang, H., Kim, S., Ko, S., 2015. Fabrication of amorphous curcumin nanosuspensions using beta-lactoglobulin to enhance solubility, stability, and bioavailability. *Colloids Surf. B: Biointerfaces* 127, 114–121.
- Chen, K., Yang, R., Shen, F.Q., Zhu, H.L., 2020. Advances in pharmacological activities and mechanisms of glycyrrhizic acid. *Curr. Med. Chem.* 27, 6219–6243.
- Choi, J.S., Park, J.S., 2017. Development of docetaxel nanocrystals surface modified with transferrin for tumor targeting. *Drug Des. Devel. Ther.* 11, 17–26.
- Dhaval, M., Makwana, J., Sakariya, E., Dudhat, K., 2020. Drug nanocrystals: a comprehensive review with current regulatory guidelines. *Curr. Drug Deliv.* 17, 470–482.
- Gao, L., Liu, G., Ma, J., Wang, X., Zhou, L., Li, X., Wang, F., 2013. Application of drug nanocrystal technologies on oral drug delivery of poorly soluble drugs. *Pharm. Res.* 30, 307–324.
- Gigliobianco, M.R., Casadidio, C., Censi, R., Di Martino, P., 2018. Nanocrystals of poorly soluble drugs: drug bioavailability and physicochemical stability. *Pharmaceutics* 10, 134.
- Guo, J.J., Yue, P.F., Lv, J.L., Han, J., Fu, S.S., Jin, S.X., Jin, S.Y., Yuan, H.L., 2013. Development and in vivo/in vitro evaluation of novel herpetrine nanosuspension. *Int. J. Pharm.* 441, 227–233.
- Hang, L., Hu, F., Shen, C., Shen, B., Zhu, W., Yuan, H., 2021. Development of herpetrine nanosuspensions stabilized by glycyrrhizin for enhancing bioavailability and synergistic hepatoprotective effect. *Drug Dev. Ind. Pharm.* 47, 1664–1673.
- Hang, L.Y., Shen, C.Y., Shen, B.D., Yuan, H.L., 2022. Insight into the fate of intravenous herpetrine amorphous nanosuspensions by aggregation-caused quenching probes. *Chin. Chem. Lett.* 33, 4948–4951.
- He, W., Lu, Y., Qi, J., Chen, L., Hu, F., Wu, W., 2013. Food proteins as novel nanosuspension stabilizers for poorly water-soluble drugs. *Int. J. Pharm.* 441, 269–278.
- Jacob, S., Nair, A.B., Shah, J., 2020. Emerging role of nanosuspensions in drug delivery systems. *Biomater. Res.* 24, 3.
- Jin, X., Luo, Y., Chen, Y., Ma, Y., Yue, P., Yang, M., 2019. Novel breviscapine nanocrystals modified by panax notoginseng saponins for enhancing bioavailability and synergistic anti-platelet aggregation effect. *Colloids Surf. B: Biointerfaces* 175, 333–342.
- Junyaprasert, V.B., Morakul, B., 2015. Nanocrystals for enhancement of oral bioavailability of poorly water-soluble drugs. *Asian J. Pharm. Sci.* 10, 13–23.
- Kalhapure, R.S., Palekar, S., Patel, K., Monpara, J., 2022. Nanocrystals for controlled delivery: state of the art and approved drug products. *Expert Opin. Drug Deliv.* 19, 1303–1316.
- Li, J., Wang, Z., Zhang, H., Gao, J., Zheng, A., 2021. Progress in the development of stabilization strategies for nanocrystal preparations. *Drug Deliv.* 28, 19–36.
- Liu, Y., Ma, Y., Xu, J., Chen, Y., Xie, J., Yue, P., Zheng, Q., Yang, M., 2017. Apolipoproteins adsorption and brain-targeting evaluation of baicalin nanocrystals modified by combination of Tween80 and TPGS. *Colloids Surf. B: Biointerfaces* 160, 619–627.
- Long, J., Song, J., Zhang, X., Deng, M., Xie, L., Zhang, L., Li, X., 2020. Tea saponins as natural stabilizers for the production of hesperidin nanosuspensions. *Int. J. Pharm.* 583, 119406.
- Lu, Y., Wang, Z.H., Li, T., McNally, H., Park, K., Sturek, M., 2014. Development and evaluation of transferrin-stabilized paclitaxel nanocrystal formulation. *J. Control. Release* 176, 76–85.
- Lu, L., Xu, Q., Wang, J., Wu, S., Luo, Z., Lu, W., 2022. Drug nanocrystals for active tumor-targeted drug delivery. *Pharmaceutics* 14, 797.
- Ma, Y., Cong, Z., Gao, P., Wang, Y., 2023. Nanosuspensions technology as a master key for nature products drug delivery and in vivo fate. *Eur. J. Pharm. Sci.* 185, 106425.
- McGuckin, M.B., Wang, J., Ghanma, R., Qin, N., Palma, S.D., Donnelly, R.F., Paredes, A. J., 2022. Nanocrystals as a master key to deliver hydrophobic drugs via multiple administration routes. *J. Control. Release* 345, 334–353.
- Mohammad, I.S., Hu, H., Yin, L., He, W., 2019. Drug nanocrystals: Fabrication methods and promising therapeutic applications. *Int. J. Pharm.* 562, 187–202.
- Qiao, Y., Cao, Y., Yu, K., Zong, L., Pu, X., 2020. Preparation and antitumor evaluation of quercetin nanosuspensions with synergistic efficacy and regulating immunity. *Int. J. Pharm.* 589, 119830.
- Qin, M., Xin, J., Han, W., Li, M., Sui, X., Dong, H., Fu, Q., He, Z., 2022. Stabilizer-induced different in vivo behaviors for intramuscularly long-acting celecoxib nanocrystals. *Int. J. Pharm.* 628, 122298.
- Selyutina, O.Y., Polyakov, N.E., 2019. Glycyrrhizic acid as a multifunctional drug carrier - from physicochemical properties to biomedical applications: a modern insight on the ancient drug. *Int. J. Pharm.* 559, 271–279.
- Shen, B.D., Shen, C.Y., Yuan, X.D., Bai, J.X., Lv, Q.Y., Xu, H., Dai, L., Yu, C., Han, J., Yuan, H.L., 2013. Development and characterization of an orodispersible film containing drug nanoparticles. *Eur. J. Pharm. Biopharm.* 85, 1348–1356.
- Shen, B., Wu, N., Shen, C., Zhang, F., Wu, Y., Xu, P., Zhang, L., Wu, W., Lu, Y., Han, J., Wang, Y., Yuan, H., 2016. Hyperoside nanocrystals for HBV treatment: process optimization, in vitro and in vivo evaluation. *Drug Dev. Ind. Pharm.* 42, 1772–1781.
- Shen, C., Yang, Y., Shen, B., Xie, Y., Qi, J., Dong, X., Zhao, W., Zhu, W., Wu, W., Yuan, H., Lu, Y., 2018. Self-discriminating fluorescent hybrid nanocrystals: efficient and accurate tracking of translocation via oral delivery. *Nanoscale* 10, 436–450.
- Shen, C., Zhu, J., Song, J., Wang, J., Shen, B., Yuan, H., Li, X., 2020. Formulation of pluronic F127/TPGS mixed micelles to improve the oral absorption of glycyrrhizic acid. *Drug Dev. Ind. Pharm.* 46, 1100–1107.
- Shen, B., Shen, C., Zhu, W., Yuan, H., 2021a. The contribution of absorption of integral nanocrystals to enhancement of oral bioavailability of quercetin. *Acta Pharm. Sin. B* 11, 978–988.
- Shen, C., Shen, B., Zhu, J., Wang, J., Yuan, H., Li, X., 2021b. Glycyrrhizic acid-based self-assembled micelles for improving oral bioavailability of paeoniflorin. *Drug Dev. Ind. Pharm.* 47, 207–214.
- Soisuan, S., Teeranachaiidekul, V., Wongrakpanich, A., Langguth, P., Junyaprasert, V. B., 2019. Impact of uncharged and charged stabilizers on in vitro drug performances of clarithromycin nanocrystals. *Eur. J. Pharm. Biopharm.* 137, 68–76.
- Stecanella, L.A., Bitencourt, A.P.R., Vaz, G.R., Quarta, E., Silva Junior, J.O.C., Rossi, A., 2021. Glycyrrhizic acid and its hydrolyzed metabolite 18beta-glycyrrhetic acid as specific ligands for targeting nanosystems in the treatment of liver cancer. *Pharmaceutics* 13.
- Tian, Y., Wang, S., Yu, Y., Sun, W., Fan, R., Shi, J., Gu, W., Wang, Z., Zhang, H., Zheng, A., 2022. Review of nanosuspension formulation and process analysis in wet media milling using microhydrodynamic model and emerging characterization methods. *Int. J. Pharm.* 623, 121862.
- Tu, L., Cheng, M., Sun, Y., Fang, Y., Liu, J., Liu, W., Feng, J., Jin, Y., 2020. Fabrication of ultra-small nanocrystals by formation of hydrogen bonds: in vitro and in vivo evaluation. *Int. J. Pharm.* 573, 118730.
- Tucker, I.M., Burley, A., Petkova, R.E., Hosking, S.L., Penfold, J., Thomas, R.K., Li, P.X., Webster, J.R.P., Welbourn, R., Douth, J., 2021. Adsorption and self-assembly properties of the plant based biosurfactant, Glycyrrhizic acid. *J. Colloid Interface Sci.* 598, 444–454.
- Tuomela, A., Hirvonen, J., Peltonen, L., 2016. Stabilizing agents for drug nanocrystals: effect on bioavailability. *Pharmaceutics* 8, 16.
- Wang, T., Qi, J., Ding, N., Dong, X., Zhao, W., Lu, Y., Wang, C., Wu, W., 2018. Tracking translocation of self-discriminating curcumin nanocrystals following intravenous delivery. *Int. J. Pharm.* 546, 10–19.
- Wang, Z., Dai, B., Tang, X., Che, Z., Hu, F., Shen, C., Wu, W., Shen, B., Yuan, H., 2022. Fabrication and in vitro/vivo evaluation of drug nanocrystals self-stabilized pickering emulsion for oral delivery of quercetin. *Pharmaceutics* 14, 897.
- Yang, F.H., Zhang, Q., Liang, Q.Y., Wang, S.Q., Zhao, B.X., Wang, Y.T., Cai, Y., Li, G.F., 2015. Bioavailability enhancement of paclitaxel via a novel oral drug delivery system: paclitaxel-loaded glycyrrhizic acid micelles. *Molecules* 20, 4337–4356.
- Yang, H., Kim, H., Jung, S., Seo, H., Nida, S.K., Yoo, S.Y., Lee, J., 2018. Pharmaceutical strategies for stabilizing drug nanocrystals. *Curr. Pharm. Des.* 24, 2362–2374.
- Yin, T., Cai, H., Liu, J., Cui, B., Wang, L., Yin, L., Zhou, J., Huo, M., 2016. Biological evaluation of PEG modified nanosuspensions based on human serum albumin for tumor targeted delivery of paclitaxel. *Eur. J. Pharm. Sci.* 83, 79–87.
- Yue, P.F., Li, Y., Wan, J., Wang, Y., Yang, M., Zhu, W.F., Wang, C.H., Yuan, H.L., 2013. Process optimization and evaluation of novel baicalin solid nanocrystals. *Int. J. Nanomedicine* 8, 2961–2973.
- Zhao, F.Q., Wang, G.F., Xu, D., Zhang, H.Y., Cui, Y.L., Wang, Q.S., 2021a. Glycyrrhizin mediated liver-targeted alginate nanogels delivers quercetin to relieve acute liver failure. *Int. J. Biol. Macromol.* 168, 93–104.
- Zhao, X., Wang, J., Deng, Y., Liao, L., Zhou, M., Peng, C., Li, Y., 2021b. Quercetin as a protective agent for liver diseases: a comprehensive descriptive review of the molecular mechanism. *Phytother. Res.* 35, 4727–4747.
- Zingale, E., Bonaccorso, A., Carbone, C., Musumeci, T., Pignatello, R., 2022. Drug Nanocrystals: Focus on Brain Delivery from Therapeutic to Diagnostic applications. *Pharmaceutics* 14, 691.